Microcellular Foaming of Amorphous High-T_g Polymers Using Carbon Dioxide

B. Krause, R. Mettinkhof, N. F. A. van der Vegt,* and M. Wessling

Membrane Technology Group, University of Twente, P.O. Box 217, 7500 AE Enschede, The Netherlands

Received July 24, 2000

ABSTRACT: The foaming of thin (∼100 μm) polysulfone (PSU), poly(ether sulfone) (PES), and cyclic olefin copolymer (COC) films using carbon dioxide as a physical blowing agent has been studied. Microcellular foam morphologies were obtained by saturating the polymer with carbon dioxide and heating the sample above the glass transition temperature of the polymer/gas mixture after releasing pressure. The temperature range at which foaming took place was examined in detail, and the physical processes fixing the final foam morphologies were discussed. We find that the ease of plasticization of the different polymers and the CO_2 diffusion coefficient under foaming conditions determine the morphology of the foams. Nucleation and growth of cells starts at the T_g of the polymer/gas mixture; however, this process is severely inhibited by enhanced diffusion of gas from the films. The maximum cell density attainable is not determined by the ease of nucleation. Instead, CO_2 loss by diffusion to the exterior of the sample determines the maximum number of cells in the polymer. This effect, which at sufficiently high temperatures results in decreasing cell densities with increasing temperature of the foaming bath, becomes stronger for the more readily plasticized system (COC > PSU > PES) and causes an upper temperature limit where foaming stops.

1. Introduction

Microcellular foaming of glassy polymers with carbon dioxide or nitrogen used as a physical-blowing agent was first described by Martini and co-workers.[1] In general, microcellular foams are characterized by a cell size of around 10 μm and a cell density between 10^9 and 10^{15} cells/cm^3. Several techniques are developed since then to prepare microcellular foams using gases in their supercritical and nonsupercritical state as physical blowing agents. These techniques all rely on the same principle: (1) the polymer is saturated with a gaseous penetrant (blowing agent) at high pressure, (2) the polymer/gas mixture is quenched into a supersaturated state by either reducing pressure or increasing temperature, and (3) nucleation and growth of gas cells dispersed throughout the polymer sample evolves until all thermodynamic forces driving mass transport vanish. Thermoplastic polymers can be foamed using continuous extrusion methods. In this process, the gas is fed into an extruder and mixed with the polymeric melt at elevated temperatures and pressures. The polymer/gas mixture subsequently foams once it passes the die of the extruder. Noncontinuous foaming techniques have been used as well. Two alternatives should be distinguished here. The first alternative (the autoclave method), which is physically the closest one to the continuous method, consists of saturating a polymer batch with the gaseous penetrant at a temperature above the glass transition temperature of the homogeneous polymer/gas mixture. The microcellular structure is obtained by quenching pressure, either instantaneously or at a controlled rate. The second alternative, which we used in the present work, consists of saturating the polymer batch (a thin film in our experiments) at a temperature below the glass transition temperature of the mixture. After removal of the saturated polymer film from the high-pressure vessel, it is foamed during a rapid heating step at a temperature (the so-called foaming temperature) above the glass transition temperature of the mixture. It is important to note that the saturated glassy structure in this case does not foam as a result of a pressure quench. If the polymer is quickly removed from the high-pressure saturation vessel, expansion of the polymer caused by nucleation and growth of cells is inhibited by the rigidity of the glassy structure. However, during the time before the heating step is applied, carbon dioxide will desorb from the polymer film, which leads to reduced carbon dioxide concentrations near the film surfaces. The foamed films, therefore, always show dense (unfoamed) surface layers and foamed cores.

The aforementioned techniques have been used to investigate the foaming behavior of amorphous and semicrystalline glassy polymers such as poly(vinyl chloride),[2] polystyrene,[3,4] polycarbonate,[5,6] poly(methyl methacrylate),[6−8] poly(ethylene terephthalate),[9] and polysulfone.[10,11] In some cases, the influence of the gas saturation pressure and the temperature on the microcellular morphologies were interpreted in terms of classical nucleation theories. With thin polymer samples (films or sheets) such an interpretation is hampered, because mass conservation of the nucleating phase is not obeyed, i.e., carbon dioxide diffuses into the environment on the time scale during which the microcellular structure is formed. The main purpose of the present work is to investigate how (1) this phenomenon affects the cell density as a function of temperature and (2) this phenomenon depends on the plasticization of different polymeric materials.

In this work, we study the microcellular foaming process of PSU, PES, and COC. Polysulfone, poly(ether sulfone), and cyclic olefin copolymer microcellular foams are featured by improved mechanical properties[12] in

* Corresponding author: e-mail: N.F.A.vandervegt@ct.utwente.nl.

10.1021/ma001291z CCC: $20.00
Published on Web 01/17/2001

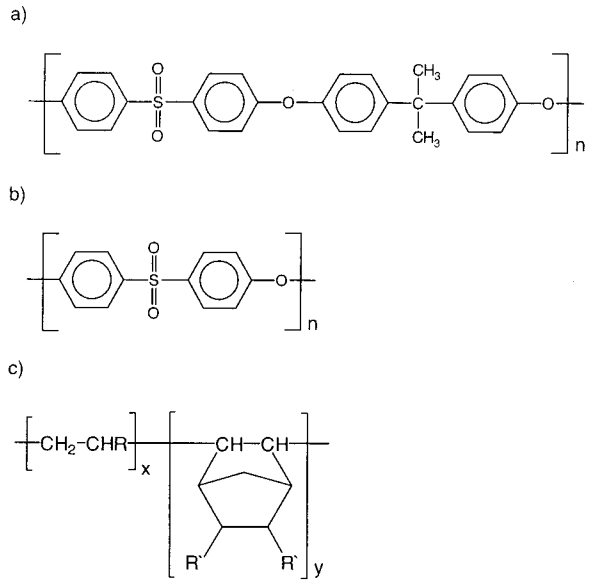

Figure 1. Chemical structures of the (a) bisphenol A polysulfone and (b) poly(ether sulfone) monomer units and (c) the cyclic olefin copolymer structure.

combination with a high thermal stability. These closed-cell foams possess very low dielectric constants and good thermal insulation properties. The work described in this paper forms the basis for the production of open-cellular foams,[13] which have numerous applications in devices to control mass transport, i.e., membranes for ultrafiltration, hemodialysis, etc.

In this article, we will show how the discontinuous microcellular foaming process described above can be used to form thin foamed polymeric films with microcellular morphologies. In the first part of our investigation (section 3.1), we show the strong impact of several process conditions on the final foam morphology. The studied parameters are optimized such that maximum cell densities, minimal cell diameters, and minimal mass densities are obtained. In the second part (section 3.2), we will present the influence of the foaming temperature on the microcellular foam morphology of the different polymers. In particular, we show that foaming of amorphous glassy polymers is only possible in a well-defined temperature window, which is set by the plasticization behavior of the polymer/gas mixture. Four different temperature zones are identified, and their typical characteristics are presented as well as the influence of different mechanisms controlling the foam formation process over the entire temperature range. It will be shown that the characteristics of the cell density vs temperature graphs are determined by bubble nucleation for strong plasticization resistant polymers and by deterioration of nuclei caused by diffusion in easily plasticized polymers.

2. Experimental Section

2.1. Materials. Three commercially available polymer samples, bisphenol A polysulfone (PSU), type Udel P-3500, received from Amoco Chemicals, Belgium, poly(ether sulfone) (PES) type 7300 P, received from Sumitomo Chemicals, Japan, and a cyclic olefin copolymer (COC), type Topas COC 6013, received from Ticona, Germany, are used in this work. The chemical structures of the three different polymers are shown in Figure 1. Tetrahydrofuran (THF), dimethylformamide (DMF), *N*-methylpyrrolidone (NMP), cyclohexane, hexane, and ethanol were purchased from Merck (analytical grade) and used as received. Carbon dioxide was purchased from Praxair having purity a larger than 99.99%.

Table 1. Polymer Film Properties

sample	M_n (kg/mol)	M_w (kg/mol)	M_w/M_n	T_g (°C)	density (g/cm^3)
PES	M_{p1}: 173 kg/mol; M_{p2}: 622 kg/mol			228	1.39
PSU	33.9	67.1	1.98	193	1.26
COC	54.0	84.5	1.57	139	1.01

Table 2. Dual Mode Sorption Parameters of CO_2 for the PES, PSU, and COC Films at 25 °C

sample	k_D (cm^3(STP)/cm^3 (polymer)/bar)	C_h' (cm^3(STP)/cm^3 (polymer))	b (bar^{-1})
PES	0.308	39.02	0.1257
PSU	0.101	41.88	0.0866
COC	0.072	40.43	0.0178

2.2. Film Preparation. The polymers are used as received without further purification for film formation. Solutions of PSU, PES, and COC were prepared by dissolving 20 wt % polymer in THF, NMP, and cyclohexane, respectively. Thin films of around 100 μm thickness were formed by solution casting on a glass plate. The casted PSU and COC films were dried in a nitrogen atmosphere at room temperature for 24 h, whereas the PES film was dried in a nitrogen atmosphere at 75 °C for 4 h. Subsequently, the homogeneous dense films were removed from the glass plate with the help of a small amount of water and further dried under vacuum (Heraeus VT 6060M in combination with an Edwards RV3 rotary vane pump) at 30 (PSU), 100 (COC), and 150 °C (PES) for several weeks to remove the last traces of solvents. These films were analyzed using gas chromatography (headspace technique) to determine remaining THF and cyclohexane and elemental analysis (N) to determine remaining NMP traces. The remaining solvent concentrations were all found smaller than 0.03 wt %. The presence of residual solvent traces in the polymer film can cause open-cell formation.[13]

2.3. Polymer Film Characterization. Absolute molecular weights and molecular weight distributions of the PSU and COC samples were determined by gel permeation chromatography (GPC) using a system equipped with Waters μ-Styragel columns (10^6, 10^5, 10^4, 10^3), a Waters 510 HPLC pump with DMF (PSU and PES) and cyclohexane (COC) as the mobile phase, and a Waters 411 RI detector in combination with a Chromatix KMX-6 LALLS detector. The PES sample showed a bimodal molecular weight distribution. Because of this, we only determined the molecular weight at the peak maximum (M_p) relative to polystyrene using the described analytical setup. A Perkin-Elmer differential scanning calorimeter DSC7 was used to determine the glass transition temperature (T_g) of the prepared films. The T_g was obtained from the second run, using a heating rate of 20 K/min. Density measurements on the films at 25 °C were performed using a Micromeritics AccuPyc 1330 pycnometer. The molecular weight values, the polydispersities, the glass transition temperatures, and the mass densities of the prepared polymer films are summarized in Table 1.

The equilibrium sorption of carbon dioxide into the three different polymer films was measured using a dual volume setup similar to the one described by Koros et al.[14,15] The equipment used and the experimental procedure of the sorption measurements is described elsewhere.[16] Sorption isotherms for the pressure range up to 50 bar at 25 °C were determined for all films. The obtained equilibrium data points were fitted by the dual mode sorption model.[17] The model parameters are given in Table 2. Figure 2 shows the carbon dioxide sorption isotherms for the polysulfone, poly(ether sulfone), and cyclic olefin copolymer samples at 25 °C. Using the dual mode sorption parameters, the extrapolated absorbed amount of carbon dioxide at 50 bar and 25 °C in the PSU film amounts to 39.1 cm^3 (STP)/cm^3 (polymer). The PES sample exhibits an approximately 25% higher sorption capacity for carbon dioxide at 50 bar and 25 °C, which amounts to 49.1 cm^3 (STP)/cm^3 (polymer), whereas the COC films shows a

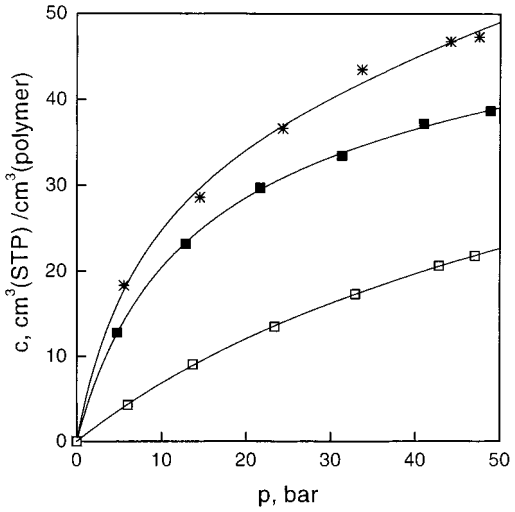

Figure 2. Sorption isotherm for the sorption of CO_2 in PSU (■), COC (□), and PES (*) at 25 °C. (Symbols are experimental values, and lines represent the dual mode sorption model fit.)

significantly lower sorption capacity, which amounts to 22.7 cm^3 (STP)/cm^3 (polymer).

2.4. Microcellular Foam Formation (Pressure Cell Technique). The prepared polymer films were cut into 4 cm × 4 cm pieces and placed in a pressure vessel connected to a carbon dioxide cylinder. The samples were then saturated with carbon dioxide at room temperature (23−25 °C) and elevated pressure (10−50 bar). Subsequently, the carbon dioxide was quickly released from the pressure vessel (within 1 s). After removing the gas-saturated polymer film from the pressure vessel, the sample was immersed in a glycerol bath maintained at the desired temperature during a fixed time (foaming time). The foamed samples were next quenched in an ethanol/water (1 + 1) mixture, washed in ethanol for a least 1 h, and dried under vacuum (Heraeus VT 6060M in combination with an Edwards RV3 rotary vane pump) at 30 °C for 24 h to remove traces of ethanol and water.

2.5. Microcellular Foam Characterization. The foamed polymer films were characterized to determine their mass densities, cell densities, cell size distributions, and thickness of the dense outer skin. The mass densities of the foamed polymer samples were analyzed by using the flotation weight loss method (ASTM D-792) with hexane (PES/PSU) and ethanol (COC) as liquid. Liquid uptake in the foamed sample could not be observed during the measurement, which process would overestimate the true density. The obtained mass densities are average values of the entire polymer sample, i.e., the foamed core part including the integral dense skin.

The microcellular morphologies of the foamed samples were investigated using a Joel TM220A scanning electron microscope (SEM). The samples were freeze fractured in liquid nitrogen and sputter coated (Balzers/Union 040) with gold at an argon pressure of 0.1 Torr for 10 min at a current of 15 mA. The cell densities were determined from SEM micrographs using a procedure described previously by Kumar et al.[2] In this procedure, only the number of cells inside a window located in the center part of the foam was counted. The cell size was obtained by measuring the maximum diameter of each cell perpendicular to the skin. To determine the cell size distribution, the size of at least 150 cells in the core part of the cross section of the fractured foam sample was measured. The thickness of the integral skin was determined using the method described by Kumar and Weller.[18]

3. Results and Discussion

Applying the discontinuous pressure cell technique, several variables that can influence the foam morphology need to be optimized and fixed to elaborate the effects of changing just one of these on the microcellular foam morphology. The important variables in our process are the following: (a) foaming time: residence time of the gas saturated sample in the heating bath; (b) saturation time: residence time in the CO_2 pressure vessel; (c) transfer time: the time elapsed between removing the saturated polymer sample from the pressure vessel and the heating step; (d) saturation pressure: the CO_2 pressure in the saturation vessel; (e) foaming temperature: the temperature of the foaming bath. The influence of these factors on the foam morphology was systematically studied to get a thorough understanding of the foaming process itself. The variables were optimized to obtain homogeneous cell size distributions, maximum cell densities, and minimum mass densities.

The optimization experiments were performed using PSU films. The obtained results can be transferred to the other polymer films investigated, because of similar physical and mechanical properties as well as shape. In section 3.1 the experimental results of the variables (a)−(d) are presented. Next, the influence of the foaming temperature is investigated by fixing (a)−(d) at their optimized values. In the first part of section 3.2, the influence of the saturation pressure and the foaming temperature is investigated for PSU samples. In the second part of this section, we show that the extent to which carbon dioxide plasticizes the polymer determines optimum temperature windows for foaming.

3.1. Optimization of the Foaming Process. (a) Foaming Time. Since heat and mass transport phenomena control the foaming process, the foaming time is an important parameter. Experiments were performed with PSU samples, which were saturated with CO_2 for 2 h at 50 bar. After a rapid release of the pressure, the samples were immersed in the heating bath at 180 °C for 5−60 s. The cell densities as well as the mass densities showed constant values for foaming times between 5 and 60 s, indicating that the cell growth process occurs at times smaller than these, and coarsening phenomena do not occur. Kumar et al.[5,19] showed a strong influence of the foaming time on the cell density, using the pressure cell technique applied to 1.5−2.0 mm thick polycarbonate and poly(vinyl chloride) samples. Apparently, here, heat transfer times are much larger compared to the times in our experiments performed with ∼100 μm thick films. Time-dependent temperature profiles for polymer films with a thickness of 100 μm and 2 mm were calculated, and the results show that the films reach the temperature of the foaming bath after 0.05 and 15 s, respectively. In these calculations a constant thermal diffusion coefficient of 2×10^{-7} m^2/s was used.[20]

(b) Saturation Time. To compare the cell densities of different foamed polymer samples, a homogeneous cell size distribution across the fractured surface is necessary. This can only be obtained when a homogeneous carbon dioxide concentration profile across the film has established in the saturation step. Concentration gradients result in asymmetric cell densities and cell size distributions across the film. The experiments described in section (a) were performed by saturating the samples for 2 h. These foams showed homogeneous cell distributions. Additional experiments were performed in which PSU films were saturated during several time intervals between 20 and 180 min at room temperature, using 50 bar carbon dioxide pressure. Using a short but constant transfer time (10 s), the

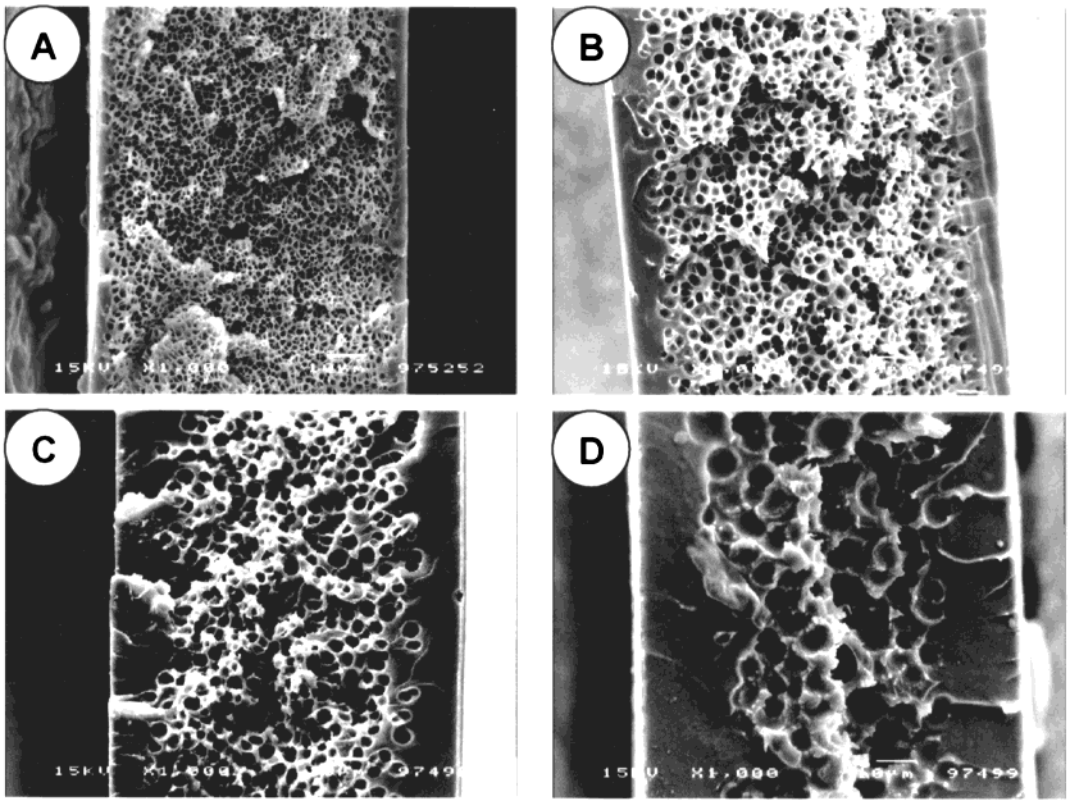

Figure 3. SEM micrographs of foamed PSU films as a function of transfer time, viz., (A) = 1 min, (B) = 5 min, (C) = 10 min, and (D) = 20 min. Magnification: 1000; the white horizontal bar indicates 10 μm.

saturated films were foamed at 180 °C for 30 s. The films saturated longer than 60 min did no longer show changes in the cell density of the foam. This result was confirmed by calculating the time-dependent concentration profile in the film using a diffusion equation for plane sheets derived by Crank[21] assuming an uniform initial CO_2 distribution and equal surface concentration. In these calculations a constant diffusion coefficient of 1×10^{-12} m^2/s was used, which was determined by Wang and Kamiya[22] for carbon dioxide in polysulfone at 25 °C at infinite dilution. In the following experimental series, all films were saturated for at least 2 h to ensure a complete saturation of the PSU film.

(c) Transfer Time. Carbon dioxide desorption from the film surface during the transfer step between the pressure cell and the heating bath results in a dense skin on the foamed polymer films. This phenomenon was modeled by Wessling[10] and Kumar and Weller.[18,23] In our experiments we have chosen a foaming temperature close to the glass transition temperature of the pure polymer, in contrast to the foaming experiments described by Wessling, which were performed far below the glass transition temperature of the pure polymer. Our choice of the foaming temperature leads to a significantly reduced skin formation. Saturation of PSU films took place at room temperature with 50 bar carbon dioxide pressure for 2 h. The transfer time was varied between 0.5 and 20 min, after which the samples were foamed at 180 °C for 30 s. A linear relation between the average layer thickness of the skin and the square root of the desorption time was obtained, in agreement with the results presented by Wessling.[10] To visualize this effect, SEM micrographs for foamed P-3500 films are shown in Figure 3 for different transfer times, i.e., 1, 5, 10, and 20 min. It is clearly visible that with increasing transfer time the thickness of the integral skin increases. In addition, the cell size increases with increasing transfer time. This is caused by the reduction of the carbon dioxide content of the film, which we will study in more detail in the next section.

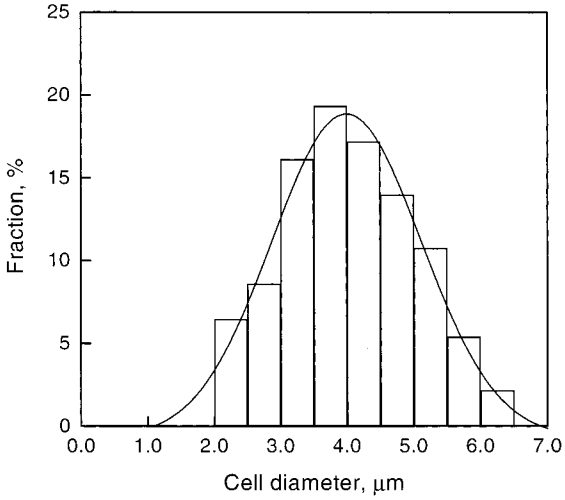

Figure 4. Cell size distribution in a foamed PSU film. The film was saturated with 10 bar carbon dioxide at 25 °C and foamed at 180 °C for 30 s. A Gaussian fit with an average value $\bar{d} = 4.0$ μm and variance $\sigma_d^2 = 5.0$ μm^2 was performed through the data.

(d) Saturation Pressure. The dissolved amount of carbon dioxide is a crucial quantity which significantly affects the cell density and the average cell diameter as already observed by varying the transfer time (Figure 3). To investigate the dependence of these properties on the carbon dioxide concentration in the polymer, PSU films were saturated for 2 h at different carbon dioxide pressures and subsequently foamed at 180 °C for 30 s. A typical cell size distribution for a saturation pressure

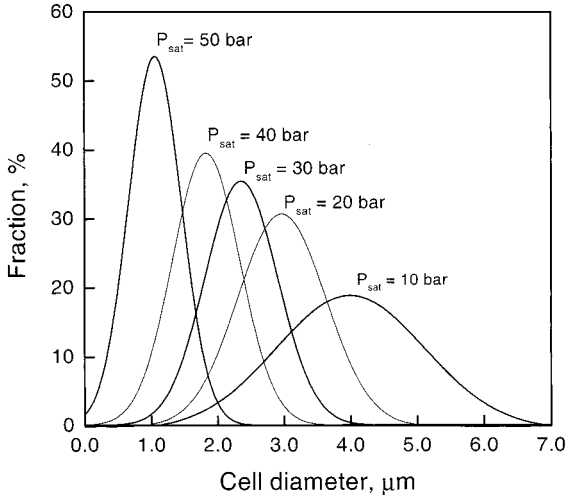

Figure 5. Cell size distributions of foamed PSU films saturated at different carbon dioxide pressures (P_{sat}) at room temperature. The foaming process was performed at 180 °C for 30 s.

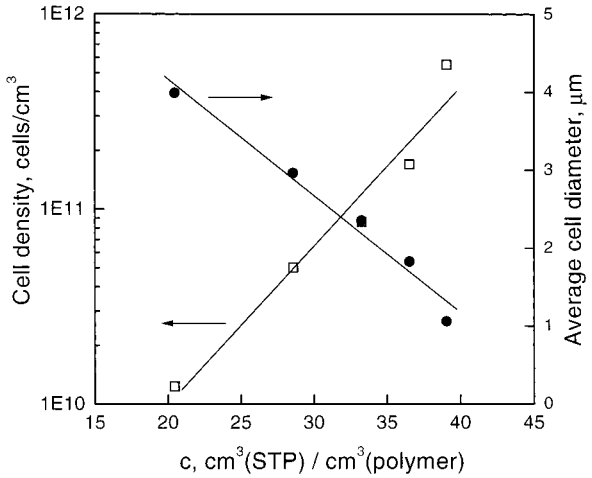

Figure 6. Cell size distributions and the average cell diameter of foamed PSU films saturated at different carbon dioxide pressures at room temperature. All films were foamed at 180 °C for 30 s.

(P_{sat}) of 10 bar is shown in Figure 4. The cell sizes obey a Gaussian distribution with average $\bar{d} = 4.0\ \mu$m and variance $\sigma_d^2 = 5.0\ \mu m^2$. The cell size distributions at different saturation pressures are shown in Figure 5. It is clearly visible that, with increasing carbon dioxide concentration, both the average diameter and the variance of the distributions decrease. In Figure 6, we have plotted the average cell diameter and the cell density vs the CO_2 concentration in the polymers. The cell density apparently grows exponentially with the CO_2 concentration; the average cell diameter decreases linearly. Itoh et al.[11] investigated the influence of the saturation pressure on the cell diameter and cell density for polysulfone, Sumilite FS-1200. The foaming process took place in a heated air oven to induce foaming. Because of the slower heat transfer in their experiments and a different method for measuring the cell diameter, direct comparison to our results is questionable. Despite this, these authors observed similar trends at various CO_2 concentrations. Handa and Zhang[24] performed similar investigations for PMMA. Their results show comparable cell size and cell density patterns with the dissolved carbon dioxide concentration.

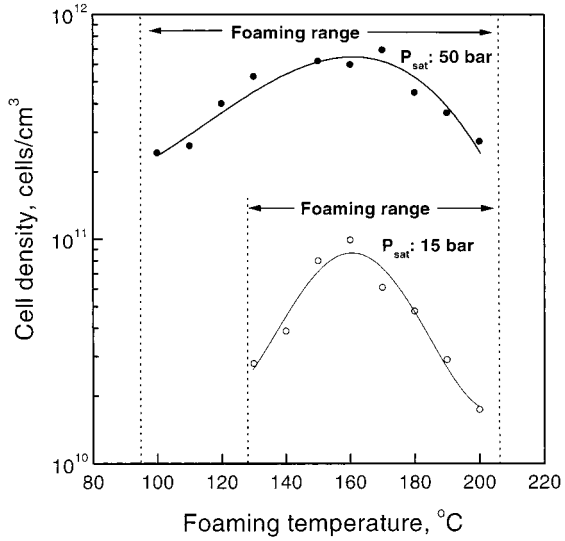

Figure 7. Cell density of PSU for different foaming temperatures saturated with 15 bar (○) and 50 bar (●) carbon dioxide for 2 h at room temperature. Foaming times of 30 s were used. The dotted lines confine the foaming temperature range in which foam formation is observed.

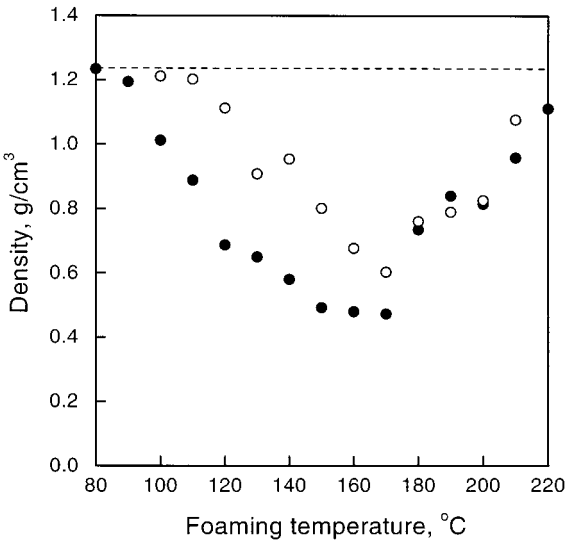

Figure 8. Mass densities of PSU for different foaming temperatures saturated with 15 bar (○) and 50 bar (●) of carbon dioxide for 2 h at room temperature. Foaming times of 30 s were used.

3.2. Influence of the Foaming Temperature. Since foaming can only take place above the T_g of the polymer/gas mixture, the foaming temperature is an important parameter to control foam morphology. To investigate the influence of the foaming temperature and the dissolved carbon dioxide concentration simultaneously, PSU samples were saturated at 15 and 50 bar for 2 h at room temperature and foamed for 30 s at temperatures between 90 and 220 °C.

The cell and mass densities for the two saturation pressures are plotted in Figures 7 and 8 vs the foaming temperature. From the cell density curve in Figure 7, it can be seen that no foam structure can be obtained below a foaming temperature of 95 and 125 °C at 50 and 15 bar CO_2 saturation pressure, respectively. This is confirmed by the mass density pattern in Figure 8, which shows no density change below these temperatures. The temperature at which foaming starts shifts to lower values with increasing CO_2 concentrations. This

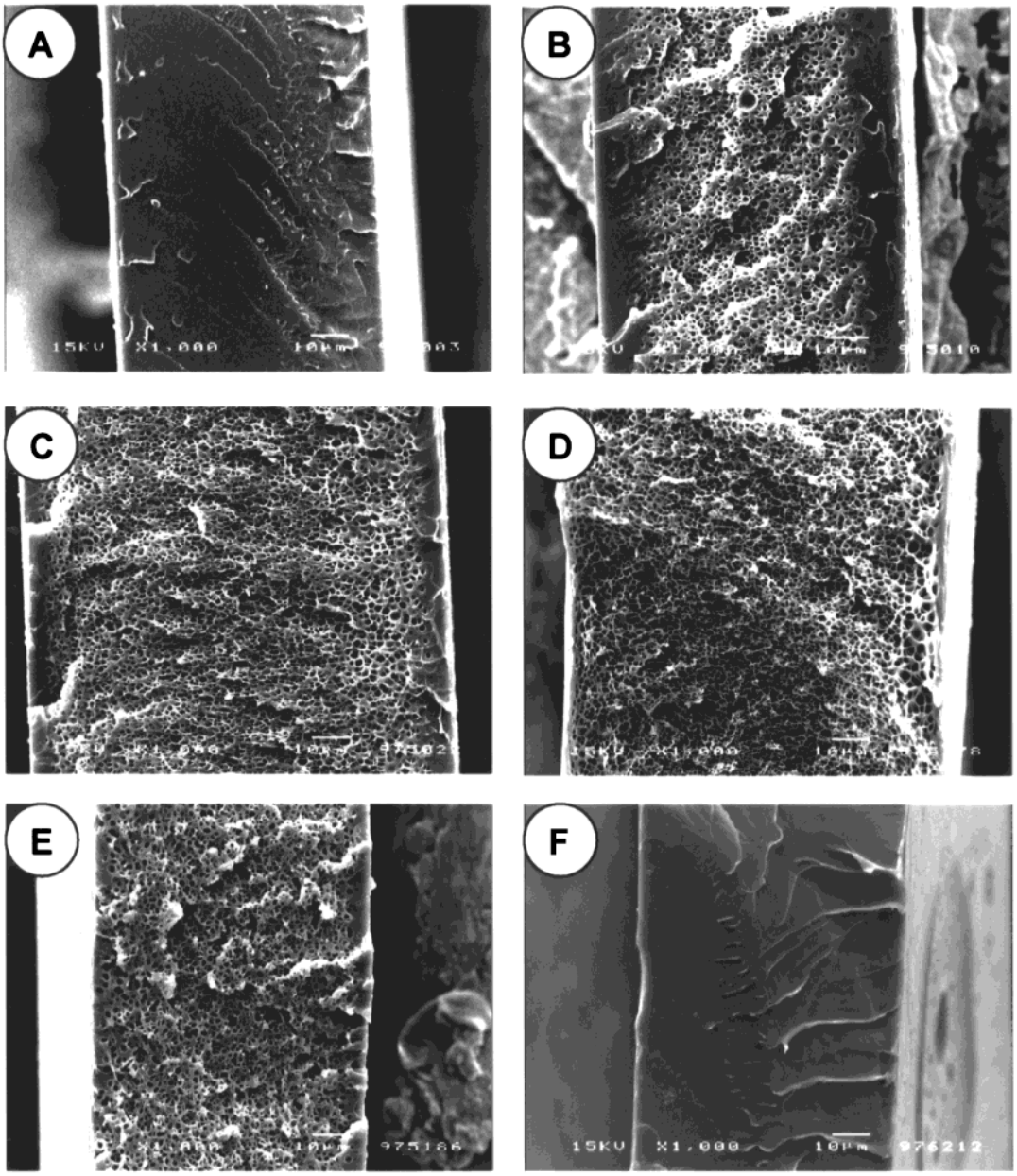

Figure 9. SEM micrographs of PSU films saturated with 50 bar and foamed at 70 (A), 100 (B), 130 (C), 160 (D), 190 (E), and 210 °C (F). Magnification: 1000; the white horizontal bar indicates 10 μm.

effect is directly related to the glass transition depression, which will be discussed later.

In addition to the lower bound temperature limit, an upper bound limit is observed. Above this temperature, which equals approximately 205 °C, foam formation can no longer be observed. This limiting temperature is 12 °C above the T_g of the pure polymer. The films, if foamed above this limiting temperature, are transparent after they are removed from the heating bath and show approximately the same density as the unfoamed polymer films. The density discrepancies in the foaming temperature range between 210 and 220 °C are due to deformation of the film samples hampering accurate measurements of the mass density. Scanning electron micrographs of the microcellular morphologies at (i) the lower temperature limit, (ii) elevated temperatures, and (iii) the upper bound temperature limit are shown in Figure 9. The PSU samples shown here were saturated with CO_2 at 50 bar and 25 °C prior to foaming. From this point on, we will refer to the lower and upper bound temperatures as T_{lower} and T_{upper}, respectively.

In between the lower and upper bound temperatures, T_{lower} and T_{upper}, the cell density curve passes through a maximum and the mass density curve passes through a minimum. The temperature, T_{max}, where the maximum of the cell density appears, is independent of the saturation pressure and is located at ca. 160−170 °C. The absolute values of the cell density, however, differ very much from each other, as expected (section 3.1.d). At exactly the temperature region where the cell density passes a maximum, the mass density pattern passes a minimum.

Kumar and Weller[5] reported the dependence of the cell density on the foaming temperature for polycarbonate. Their graphically presented data of the cell density dependence on the foaming temperature are comparable with the pattern we presented in Figure 7; viz., the cell density increases with increasing foaming temperature, reaches a maximum, and decreases by further increase of the foaming temperature. However, the maximum

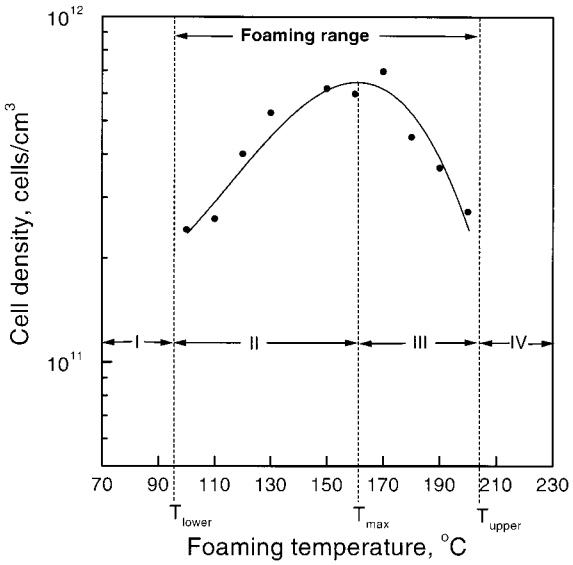

Figure 10. Representation of the cell density dependence on the foaming temperature of PSU films, saturated with 50 bar of carbon dioxide for 2 h at room temperature. Foaming times of 30 s were used.

foaming temperature investigated by Kumar and Weller was only 10 °C above the glass transition temperature of the polymer, which might not be far enough (below T_{upper}) to observe the phenomenon of the disappearance of the cellular structure. No physical interpretations of the trends were given by these authors. Handa and Zhang[24] performed foaming experiments with PMMA using carbon dioxide as physical blowing agent. Similar to Kumar and Weller, their foaming temperatures were also restricted to temperatures below T_{upper}. The observed cell density data levels off at higher foaming temperatures, and Handa and Zhang ascribe this observation to cell coalescence. In the following we will show that the observed trend can be explained differently.

By analyzing the cell density and mass density patterns (Figures 7 and 8), one can distinguish between four different zones (I−IV) graphically represented in Figure 10. We will discuss these below in consecutive order:

I. $T_{foam} < T_{lower}$: Below the lower bound temperature limit, the polymer/gas mixture is in a glassy state. The mechanical properties of the vitreous state avoid expansion of the polymer. To confirm that foaming starts exactly at the T_g of the polymer/gas mixtures, T_{lower} was determined at various CO_2 concentrations and then extrapolated back to zero concentration. The zero concentration temperature must then resemble the glass transition temperature of the pure polymer. PSU films were saturated for 2 h at different pressures, viz., 10, 15, 20, 30, 40, and 50 bar. Subsequently, the carbon dioxide pressure was released quickly, and each of the samples was immersed in a heating bath for 30 s. By increasing the temperature of the heating bath, the temperature at which foaming of the sample just became visible could be determined. At this transition, the sample turns from transparent into white. In addition, SEM micrographs of the sample were prepared to confirm the formation of cells. Typical SEM micrographs to determinate the glass transition are shown in Figure 11. Clearly, cell formation can be seen at 150 and 100 °C for 10 and 50 bar carbon dioxide pressure, respectively. The glass transition temperature was defined as the average of the two adjacent temperature values at which the transparent-to-white transition just did and did not occur. The dependence of the glass

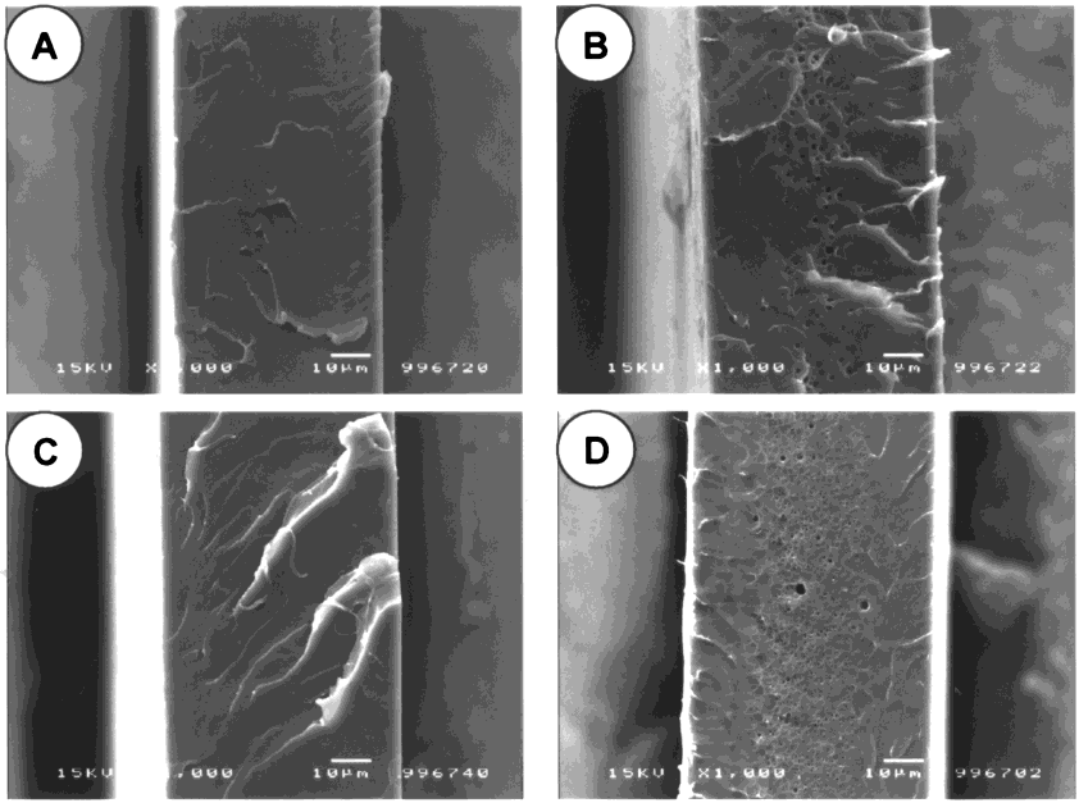

Figure 11. SEM micrographs of PSU films saturated with 10 bar (A, B) and 50 bar (C, D) of carbon dioxide and foamed at 140 (A), 150 (B), 90 (C), and 100 °C (D). Magnification: 1000; the white horizontal bar indicates 10 μm.

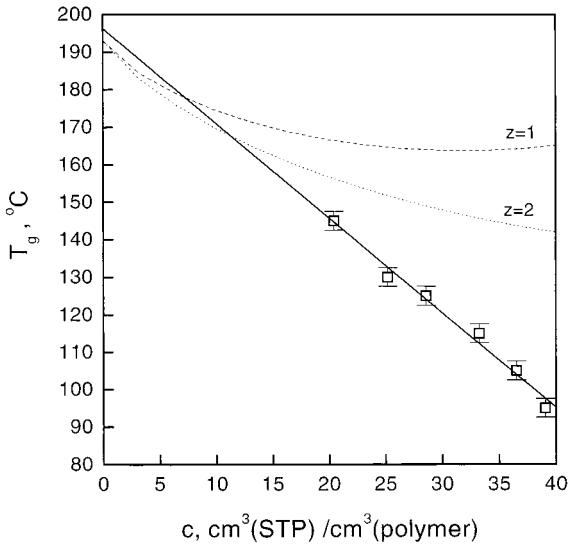

Figure 12. Glass transition temperature of PSU as a function of the carbon dioxide concentration (The straight line represents a least-squares fit of the experimental data.) The dashed ($z = 1$) and the dotted ($z = 2$) lines represent the Chow model[27] where z is the lattice coordination number.

transition temperatures of PSU on the dissolved carbon dioxide concentration is shown in Figure 12. The data points were fitted with a linear equation,

$$T_g = T_g^0 - Ac \qquad (1)$$

where T_g represents the actual glass transition temperature of the polymer/gas mixture, T_g^0 the glass transition temperature of the polymer free of carbon dioxide, c the equilibrium concentration of the dissolved carbon dioxide in the polymer, and A an empirical plasticization parameter typical for this polymer/penetrant system. Least-squares fitting of the data resulted in a value for A of 2.526 K/(cm^3 (STP)/cm^3 (polymer)). The axis intercept in Figure 12 describes the glass transition temperature of the pure, carbon dioxide free, polymer and equals 196 °C. From DSC experiments (Table 1) a glass transition temperature of 193 °C was obtained, which is in excellent agreement with the extrapolated value. The linear fit, eq 1, has proven to accurately describe the T_g depression of various polymers in independent experiments.[25,26] The model proposed by Chow[27] was used to predict the T_g of the polymer/gas mixture, and the results are shown in Figure 12. The calculations are performed using Δc_{pp} = 201 J/(kg K) for the specific heat change at the glass transition temperature for polysulfone determined by Itoh et al.[11] and a lattice coordination number (z) of 1 (dashed line) and 2 (dotted line).[28] The T_g^0 in the Chow model is the one we determined with DSC (Table 1). The calculations do not predict the experimental determined T_g, which was also seen by Itoh et al.

II. $T_{lower} \leq T_{foam} \leq T_{max}$: Foaming occurs, and the cell density reaches a maximum at T_{max}, whereas the mass density reaches a minimum value at T_{max}. In this temperature zone, the proces of nucleation and growth of cells determines the final foam morphology. The cell density appears to be exponentially related to the temperature of the foaming bath, which is common in homogeneously nucleating systems.[29] Kumar and Weller,[5] who studied the foaming of polycarbonate, observed similar behavior.

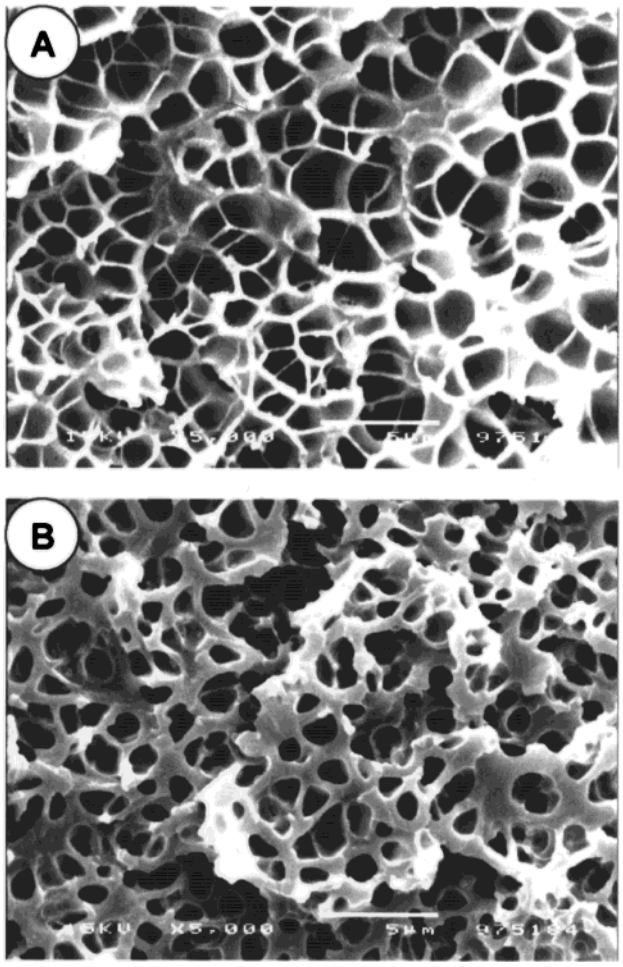

Figure 13. SEM micrographs of PSU films saturated with 50 bar of carbon dioxide for 2 h at room temperature and foamed for 30 s at 180 (A) and 200 °C (B), respectively. Magnification: 5000; the white horizontal bar indicates 5 μm.

III. $T_{max} < T_{foam} < T_{upper}$: In this temperature zone, the cell density decreases until the upper limit, T_{upper}, is reached, where the formation of a microcellular structure can no longer be observed. At temperatures between T_{max} and T_{upper}, SEM micrographs show decreasing cell sizes and increasing thickness of cell walls (cf. Figure 13). Therefore, the decrease in cell density cannot be explained by cell coalescence but must be explained by loss of CO_2 from the thin films before significant growth of cells occurs. Whereas diffusion of CO_2 to the exterior phase is expected in zone II as well, here the system apparently is plasticized sufficiently strong that CO_2 loss prevails over cell growth. Microscopically, the strong driving forces at small spatial scales will always facilitate cell growth; however, the time scale relevant for the growth process apparently is long enough for the CO_2 molecules to next move in the direction of the macroscopic gradient that points toward the exterior of the film. During this transient time, the polymer matrix surrounding the gas cells is in the rubbery or melt state due to the significant amount of dissolved CO_2. We note at this point that the term "plasticization" used in this context refers to enhanced mobility of the monomer units, which is caused by (1) the dissolved CO_2 molecules and (2) the large thermal energy unit k_bT. As a result of both, the CO_2 diffusion coefficient increases strongly.

Above, we hypothesized that the maximum in cell density is a result of two competing processes. At T_{foam}

$= T_{max}$, the mass transport resistance of the plasticized polymer phase has dropped to an extent such that the rate of penetrant loss is competitive to the cell growth rate. At $T_{foam} > T_{max}$, the process of penetrant loss prevails, and diffusion of the carbon dioxide to the outside of the polymeric material controls the process. Of course, T_{max} will be different when different polymers are considered, but we believe that the location of T_{max} cannot be predicted on the basis of the T_g of the polymer only. Its value will be fully determined by the extent in which dissolved CO_2 plasticizes the system.

IV. $T_{foam} \geq T_{upper}$: No foamed morphology is obtained if the gas-saturated polymer is immersed in a heating bath with a temperature above T_{upper}. The mass density of the obtained samples is close to the density of the pure polymer. In this zone, the foaming temperature is above the glass transition temperature of the pure polymer. Under this experimental condition, cells, initially nucleated in the system, have disappeared after the foaming experiment is completed. Most likely, cells cannot grow to large sizes because CO_2 diffuses to the exterior phase under the strong plasticizing conditions. Because the pure polymer, which remains after foaming, is in a melt state, the small cells that have been formed will disappear. In contrast, when T_{foam} is below T_g^0 (zone II and III), the formed cells are locked in by the surrounding glassy matrix. The exact value of T_{upper} will depend on the polymer properties, such as the melt viscosity and the molecular weight, and therefore can vary from one polymer to another. Preliminary results showed that T_{upper} is also a function of the foaming time. In a following paper we will show that amorphous low-T_g polymers can be foamed at temperatures far above the T_g of the pure polymer; i.e., large transient values for $T_{upper} - T_g$ are observed.

Strong and Weak Plasticizing Systems. Our interpretation of plasticization phenomena, giving rise to a maximum in the cell density vs the foaming temperature (Figure 7), can be validated by investigating polymer systems that are less susceptible or, alternatively, more susceptible to plasticization effects occurring at elevated temperatures in comparison to PSU. As a less plasticization susceptible system, we have chosen PES whereas COC was taken as a stronger plasticization susceptible system. The plasticization resistant system should show a shift of T_{max} to higher temperatures (closer to T_g^0), whereas the plasticization susceptible system should show a shift to lower temperatures (further from T_g^0).

A measure of the plasticization resistance is the glass transition depression induced by dissolved CO_2. In Figure 14, we have plotted the T_g for PES, PSU, and COC dependent on the dissolved carbon dioxide concentration. The T_g's were determined from the transparent-to-white transitions in foaming experiments as described above. PES shows the highest and COC the lowest resistance for CO_2-induced plasticization. This trend is reflected by the plasticization parameter A. In Table 3 the plasticization parameters as well as a comparison of the extrapolated T_g's (obtained from Figure 14) with T_g's measured by DSC are presented. The glass transition temperatures are in good agreement to each other and show the accuracy of this method to determine the glass transition temperature as well as the glass transition temperature depression. To emphasize the difference in plasticization of the three polymers, we show the glass transition temperature depression of the three polymers dependent on dissolved CO_2 concentration in Figure 15.

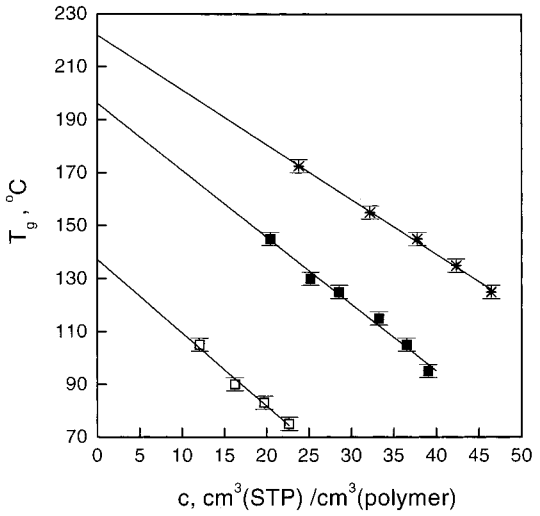

Figure 14. Glass transition temperature of PSU (■), COC (□), and PES (*) dependent on the dissolved amount of carbon dioxide.

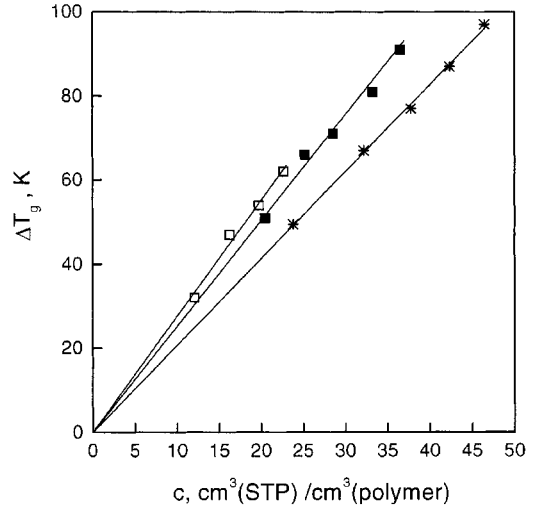

Figure 15. Glass transition temperature depression of PSU (■), COC (□), and PES (*) dependent on the dissolved amount of carbon dioxide.

Table 3. Plasticization Parameter and Glass Transition Temperature Data of PES, PSU, and COC Films

sample	A, K/(cm^3 (STP)/cm^3 (polymer)	T_g(extrapolated), °C	T_g(DSC), °C
PES	2.07	222	228
PSU	2.53	196	193
COC	2.76	137	139

Although the glass transition depressions merely reflect changes in the chain dynamics of the polymer due to dissolved CO_2, we are confident that the difference in this property between the polymers describes the dynamic changes that occur at T_{max} as well. Recent molecular simulations[30] have indicated that the response of the monomer dynamics to changes in temperature and to changes in the number of dissolved penetrants is similar.

Figure 16 shows the cell density of PES, PSU, and COC vs the foaming temperature. The polymer samples were saturated at 50 bar CO_2 pressure for 2 h at room temperature. The dotted lines confine the foaming temperature range in which foam formation is observed.

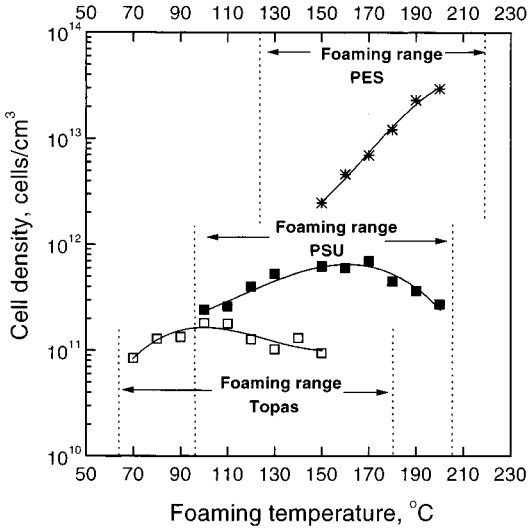

Figure 16. Cell density of PSU (■), COC (□), and PES (*) for different foaming temperatures saturated with 50 bar of carbon dioxide for 2 h at room temperature. Foaming times of 30 s were used. (Symbols are experimental values, and lines are plotted to guide the eye.) The dotted lines confine the foaming temperature range in which foam formation is observed.

For PES the cell density values in the temperature range between 125 and 150 °C are not included because these could not accurately be determined. Clearly, however, foamed samples are white and show significantly reduced mass densities in this region. At foaming temperatures above 200 °C, the cellular structure for PES could not be analyzed because of extreme deformation of the obtained films. Also in this region, films are white whereas they become transparent above 220 °C. For COC, cell density data could not be obtained in the temperature range between 155 and 180 °C because of the extreme brittleness and deformation of the foams. For all three samples, the upper temperature limit, T_{upper}, is located at exactly the temperature where the films become transparent again. Mass density measurements confirmed the locations of T_{upper}. A maximum cell density, T_{max}, for PES cannot be identified but if present lies well above the value observed for PSU. On the other hand, the maximum cell density for COC appears at 100 °C, well below the value observed for PSU. The difference, $T_{max} - T_{upper}$, for PES (based on $T_{max} \sim 200$ °C) is smaller than for PSU; i.e., the diffusional loss of CO_2 has a significantly reduced influence. In contrast to this, the difference $T_{max} - T_{upper}$ for COC is much larger than for PSU, which shows the increased plasticization effect of CO_2 for COC compared to PSU. This plasticization effect is also observed from the absolute increase in the cell density with temperature over the entire foaming range. Whereas in PES the cell density increases more than 1 order of magnitude between T_{lower} and T_{max}, in PSU the cell density increase is less than 1 order of magnitude, and COC shows the lowest cell density increase over the entire foaming temperature range. The limiting temperatures, T_{upper}, for PES, PSU, and COC are reached at approximately 220, 205, and 180 °C, respectively, which was confirmed by mass density measurements. For PES and PSU these temperatures are in the vicinity of the T_g's of the pure polymers; for COC this value lies well above its T_g. The maximum cell density for PES obtained for samples saturated at 50 bar carbon dioxide pressure are 2.9×10^{13} cells/cm^3,

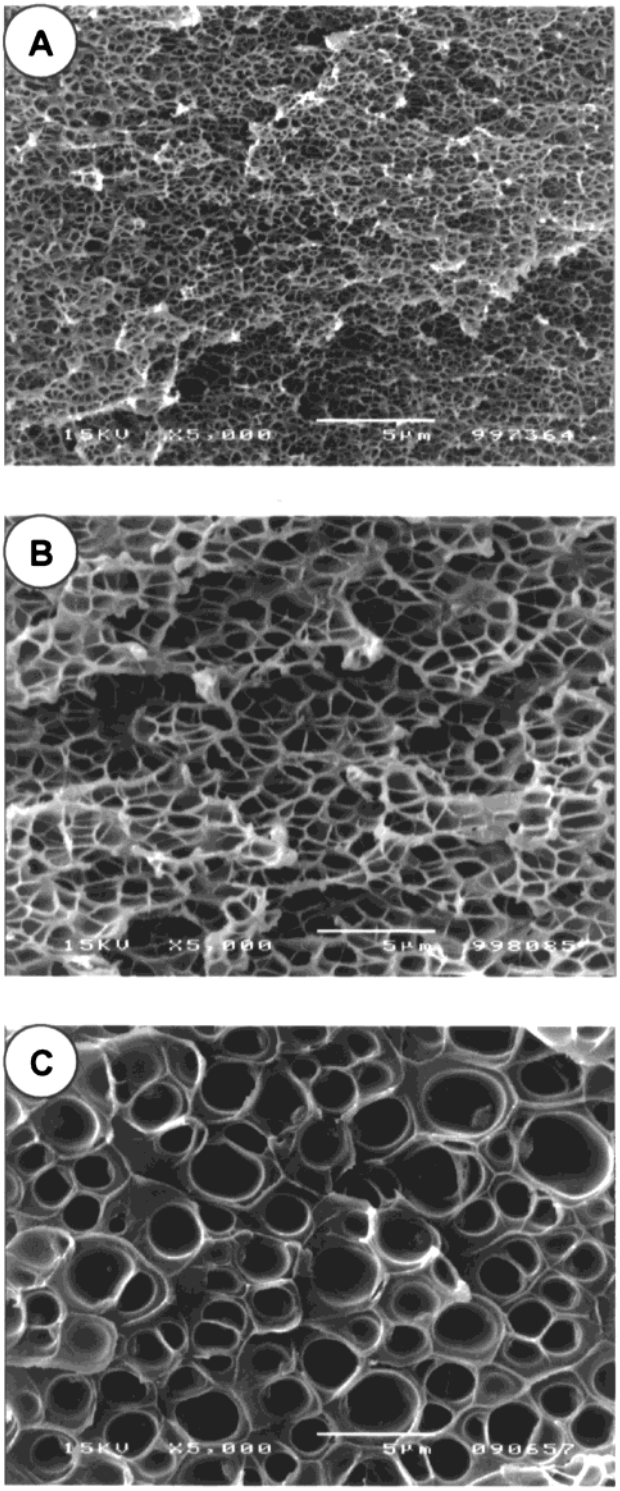

Figure 17. SEM micrographs of PES, PSU, and COC films saturated with 50 bar and foamed at 200 (A), 160 (B), and 100 °C (C), respectively. Magnification: 5000; the white horizontal bar indicates 5 μm.

which is much higher in comparison to PSU with a maximum cell density of 6.9×10^{11} cells/cm^3 and COC with a maximum cell density of 1.8×10^{11} cells/cm^3. The large differences in the cell densities pertain to the varying concentrations of carbon dioxide dissolved in the three polymers at 50 bar (Figure 2). To visualize the difference in cell density for the three polymers, SEM micrographs of foams which were prepared at $T_{foam} = T_{max}$ are shown in Figure 17.

4. Conclusions

The microcellular foaming process using carbon dioxide as physical blowing was successfully applied to polysulfone, poly(ether sulfone), and cyclic olefin copolymer. Physical properties of the polymers used as well as their gas sorption properties were characterized. The different process parameters, viz., foaming time, saturation time, transfer time, saturation pressure, and foaming temperature, were thoroughly discussed to tailor microcellular foam structures, i.e., to control the mass and cell density, the cell size distribution, and the thickness of the dense outer skin.

Four different foaming temperature regimes were identified. The different mechanisms at play at the various temperature zones were discussed as well as their influence on the final foam morphologies. It was demonstrated that foaming only takes place in the temperature range between the T_g of the polymer/gas mixture (T_{lower}) and an upper bound temperature, T_{upper}. In between these temperatures, the cell density passes through a maximum at T_{max}, because two competing processes are at play: nucleation and growth of cells and diffusion of carbon dioxide out of the plasticized polymer matrix.

To investigate the plasticization phenomena further, a poly(ether sulfone) sample and a cyclic olefin copolymer sample were foamed. The obtained results confirm that the dominating factor controlling the foam formation is the ability of the carbon dioxide to plasticize the polymer matrix.

References and Notes

(1) Martini, J. E. The Production and Analysis of Microcellular Foam. Ph.D. Thesis, Massachusetts Institute of Engineering, 1981.
(2) Kumar, V.; Weller, J. E. *Int. Polym. Process.* **1993**, *8*, 73−80.
(3) Arora, K. A.; Lesser, A. J.; McCarthy, T. J. *Macromolecules* **1998**, *31*, 4614−4620.
(4) Stafford, C. M.; Russell, T. P.; McCarthy, T. J. *Macromolecules* **1999**, *32*, 7610−7616.
(5) Kumar, V.; Weller, J. *J. Eng. Ind.* **1994**, *116*, 413−420.
(6) Blednykh, E. I.; Skripov, V. P. *Colloid J. Russ. Acad. Sci.* **1996**, *58*, 15−20.
(7) Goel, S. K.; Beckman, E. J. *Polym. Eng. Sci.* **1994**, *34*, 1137−1147.
(8) Goel, S. K.; Beckman, E. J. *Polym. Eng. Sci.* **1994**, *34*, 1148−1156.
(9) Baldwin, D. F.; Shimbo, M.; Suh, N. P. *J. Eng. Mater. Technol.* **1995**, *117*, 62−74.
(10) Wessling, M.; Borneman, Z.; Boomgaard, T. v. d.; Smolders, C. A. *J. Appl. Polym. Sci.* **1994**, *53*, 1497−1512.
(11) Itoh, M.; Kabumoto, A.; Yoshida, N. *Int. Mech. Eng. Congr. Exposition* **1994**, *53*, 139−145.
(12) Kumar, V.; Wel, M. v. d.; Weller, J.; Seeler, K. A. *J. Eng. Mater. Technol.* **1994**, *116*, 439−445.
(13) Krause, B.; Boerrigter, M. E.; Van der Vegt, N. F. A.; Wessling, M. *J. Membr. Sci.*, accepted.
(14) Koros, W. J.; Paul, D. R.; Rocha, A. A. *J. Polym. Sci.* **1976**, *14*, 687−702.
(15) Koros, W. J.; Paul, D. R. *J. Polym. Sci.* **1976**, *14*, 1903−1907.
(16) Bos, A. High Pressure CO_2/CH_4 Separation with Glassy Polymer Membranes. Ph.D. Thesis, University of Twente, 1996.
(17) Koros, W. J.; Paul, D. R. *J. Polym. Sci., Polym. Phys. Ed.* **1976**, *14*, 675.
(18) Kumar, V.; Weller, J. E. *Polym. Eng. Sci.* **1994**, *34*, 169−173.
(19) Kumar, V.; Weller, J. E.; Montecillo, R. *J. Vinyl Technol.* **1992**, *14*, 191−197.
(20) Krevelen, D. W. v. *Properties of Polymers*; Elsevier: Amsterdam, 1990.
(21) Crank, J. *The Mathematics of Diffusion*, 2nd ed.; Clarendon Press: Oxford, 1979; p 47, eq 4.17.
(22) Wang, J. S.; Kamiya, Y. *J. Membr. Sci.* **1995**, *98*, 69−76.
(23) Weller, J. E.; Kumar, V. *ANTEC* **1997**, *2*, 2037−2041.
(24) Handa, Y. P.; Zhang, Z. *J. Polym. Sci.* **2000**, *38*, 716−725.
(25) Kamiya, Y.; Mizoguchi, K.; Terada, K.; Fujiwara, Y.; Wang, J.-S. *Macromolecules* **1998**, *31*, 472−478.
(26) Chiou, J. S.; Paul, D. R. *J. Membr. Sci.* **1989**, *45*, 167−189.
(27) Chow, T. S. *Macromolecules* **1980**, *13*, 362−364.
(28) Chiou, J. S.; Barlow, J. W.; Paul, D. R. *J. Appl. Polym. Sci.* **1985**, *30*, 2633−2642.
(29) Zettlemoyer, A. C. *Nucleation*; Marcel Dekker: New York, 1969.
(30) Vegt, N. F. A. v. d.; Briels, W. J.; Wessling, M.; Strathmann, H. *J. Chem. Phys.* **1999**, *110*, 11061−11069.

MA001291Z